Frontiers in Bioscience Landmark

Front. Biosci. (Landmark Ed) **2026**; 31(6): 48694
https://doi.org/10.31083/FBL48694

Original Research

AKT-mTOR/P53 PathwayDriven RapamycinAlpelisib Efficacy in Animal Models of TIE2Mutant Venous Malformations

Yi Li[1,2,3,†], Yang He[2,4,5,†], Jian Lin[2], Tong Wang[2], Wei Wang[2], Zhencun Tang[1,*]

[1]920th Hospital of Joint Logistics Support Force, PLA, 650032 Kunming, Yunnan, China
[2]Yunnan Key Laboratory of Stomatology, Kunming Medical University, 650500 Kunming, Yunnan, China
[3]Department of Oral and Maxillofacial Surgery, The First People's Hospital of Yunnan Province, 650032 Kunming, Yunnan, China
[4]Shiyan Key Laboratory of Comprehensive Prevention and Treatment of Oral Cancer, Department of Stomatology, Taihe Hospital, Hubei University of Medicine, 442000 Shiyan, Hubei, China
[5]Institute of Oral Diseases, School of Dentistry, Hubei University of Medicine, 442000 Shiyan, Hubei, China
*Correspondence: 1845620611@qq.com (Zhencun Tang)
[†]These authors contributed equally.
Academic Editor: Graham Pawelec
Submitted: 30 November 2025 Revised: 4 March 2026 Accepted: 9 March 2026 Published: 1 June 2026

Abstract

Background: Sporadic venous malformations are a prevalent vascular anomaly in the oral and maxillofacial region. Current therapeutic strategies are associated with high recurrence rates and limited applicability in critical anatomical regions. Therefore, there is a pressing demand for more effective treatment modalities to address these challenges. **Methods**: This study utilized transcriptome sequencing to analyze samples from venous malformation patients and combined lesion tissue analysis, cell culture, and xenograft mouse models to investigate the pathogenic mechanisms and potential therapeutic approaches for venous malformations. **Results**: Our findings indicated that the primary pathological features of venous malformations include abnormal angiogenesis and excessive activation of the phosphoinositide 3-kinase (PI3K) signaling pathway. In endothelial cells with the most common pathogenic mutation, TIE2-L914F, this mutation activates the PI3K pathway, promoting cell proliferation, inhibiting normal angiogenesis, and suppressing apoptosis. Treatment with PI3K inhibitors effectively reversed these pathological changes. More importantly, the combination of rapamycin and alpelisib exhibited superior therapeutic efficacy, not only significantly inhibiting the PI3K pathway but also activating P53 expression, thereby effectively preventing disease progression. Further validation through *in vitro* 3D angiogenesis assays and xenograft mouse models confirmed the therapeutic potential of this combination. The results demonstrated a marked reduction in vessel sprouting in the 3D model and inhibited both lesion size and angiogenesis in the xenograft mouse model. **Conclusions**: This study is the first to demonstrate that the combination of rapamycin and alpelisib, through multi-target synergy, effectively inhibits the PI3K pathway and activates P53 expression, offering new insights and therapeutic options for the treatment of venous malformations.

Keywords: venous malformation; TIE2 protein; phosphatidylinositol 3-kinases; target of Rapamycin protein

1. Background

Venous malformations (VMs) represent a common category of congenital vascular anomalies that affect the skin and mucosa of the oral and maxillofacial region, while they may also involve deeper anatomical structures including skeletal muscles and internal organs [1,2]. Clinically, patients typically exhibit blue-purple, soft, and compressible vascular masses, and a considerable proportion of them may also present with symptoms such as pain, phleboliths or coagulopathy [3]. Histopathology shows characteristic features, including abnormal dilation of venous lumens, endothelial cell hyperplasia, reduced vascular smooth muscle, and adventitial fiber degeneration [4,5]. Conventional treatments include surgical resection and sclerotherapy. However, sclerotherapy can induce local inflammation and fibrosis, often requiring multiple sessions to alleviate symptoms, while surgical intervention is limited by lesion size and location and is associated with a high risk of recurrence [6–9]. Therefore, investigating the pathogenesis of VMs and identifying effective targeted therapies have significant clinical implications.

Receptor tyrosine kinase with immunoglobulin and epidermal growth factor homology domains-2(TIE2), a member of the angiopoietin (ANGPT) family, is primarily expressed in endothelial cells. Somatic mutations in TIE2 are responsible for over half of VMs, with the L914F mutation accounting for 77% of cases [10,11]. These mutations cause receptor hyperphosphorylation, leading to activation of the Phosphoinositide 3-Kinase/Protein Kinase B/Mammalian Target of Rapamycin (PI3K/AKT/mTOR) signaling pathway and subsequent VM development [12]. Additionally, activating mutations in PIK3CA are observed in approximately 50% of TIE2 mutation-negative VMs, which also promote VM formation through chronic activation of the PI3K/AKT/mTOR pathway [13]. Some patients may exhibit dual mutations in both TIE2 and Phosphatidylinositol-4,5-Bisphosphate 3-Kinase Catalytic Subunit Alpha (PIK3CA) [14].

Table 1. Experimental grouping of drugs.

Grouping	Concentration	Source	Item number
Dimethyl Sulfoxide (DMSO)	1‰	Solarbio	D8371
Rapamycin	10 nM	Laboratories	R-5000
Alpelisib	2 μM	GLPbio	GC16462
Rapamycin + Alpelisib	5 nM +1 μM	Laboratories + GLPbio	R-5000 + GC16462
Rapamycin + Ponatinib	5 nM + 50 nM	Laboratories + GLPbio	R-5000 + GC14396

Thus, dysregulation of the PI3K pathway plays a critical role in various VMs, forming the molecular pathological basis of these lesions. Although VMs associated with PIK3CA mutations have been widely investigated [12,13,15–17], the precise role of the PI3K pathway in TIE2 mutation-driven VMs remains incompletely elucidated [18–20]. This study seeks to explore the function of the PI3K pathway in TIE2-L914F mutation-related VMs and provide a theoretical foundation for developing targeted therapeutic strategies. We delivered the TIE2-L914F mutation into venous endothelial cells using a lentiviral vector and analyzed the morphological, proliferative, angiogenic, and downstream signaling alterations in these cells both *in vitro* and *in vivo*. Furthermore, we employed PI3K pathway inhibitors to determine their ability to inhibit the pathological phenotypes of VMs. Notably, we discovered that the combination of Rapamycin and Alpelisib demonstrated remarkable efficacy in treating VMs, which was further confirmed in an *in vitro* 3D angiogenesis model and a nude mouse xenograft model.

2. Methods

2.1 Cell Culture

Human umbilical vein endothelial cells (HUVECs) (iCell, iCell-h110, Shanghai, China) were isolated from human umbilical cords. All cell lines were authenticated by short tandem repeat (STR) analysis and tested negative for mycoplasma. Optical microscopy showed that endothelial cells exhibited a spindle-shaped morphology (**Supplementary Fig. 1A**). These cells were characterized by flow cytometry for surface markers (**Supplementary Fig. 1B**) and stained positive for von Willebrand factor (vWF) (**Supplementary Fig. 1C**). The cells were cultured in endothelial cell medium (ECM, iCell, Shanghai, China) containing 5% fetal bovine serum under standard conditions of 37 °C, 5% CO_2, and controlled humidity. The medium was refreshed every three days, and subsequent experiments were conducted when the cell density reached 80%–90%.

2.2 Cell Transfection

Approximately 1.5 × 10^5 HUVECs were plated in six-well plates and incubated overnight. The cells were then transfected using a lentiviral vector (Multiplicity of Infection (MOI) = 20) provided by Genechem, encoding Ubi-MCS-3FLAG-CBh-gcGFP-IRES-puromycin. Following 48 hours of transfection, the cells were cultured in ECM medium supplemented with 1.5 μg/mL puromycin (Genechem, REVG1001, Shanghai, China) for 24 hours for selection of transfected cells. Stable cell lines expressing TIE2-NC, TIE2-WT, and TIE2-L914F were established, expanded, and cryopreserved for subsequent experiments. Transfection efficiency was assessed by fluorescence microscopy and Western blot.

2.3 Drug Treatment Groups

The concentrations of experimental drugs were determined by referencing previous studies and conducting preliminary screening experiments [21,22]. The experimental design for drug combinations is presented in Table 1.

2.4 Cell Morphology Observation and Analysis

Images were captured for TIE2-NC, TIE2-WT, and TIE2-L914F cells during the logarithmic growth phase. To investigate the effects of drugs on cell morphology, images were captured after 48 hours of drug treatment. The circularity index of cells was quantified with ImageJ software (National Institutes of Health, Bethesda, MD, USA).

2.5 Cell Proliferation Assay Using CCK-8

TIE2-NC, TIE2-WT, and TIE2-L914F cells were plated in a 96-well plate coated with fibronectin at a density of 2000 cells per well, with three replicate wells. Each well was filled with 100 μL of complete ECM medium. At 0 h, 24 h, 48 h, 72 h, and 96 h, 100 μL of CCK-8 solution (GLPbio, GK10001, Montclair, California, USA) was added per well, followed by incubation at 37 °C for 2 hours. The optical density (OD) at 450 nm was determined with a microplate reader, and growth curves for the three cell types were plotted. To investigate the effects of drugs on cells, drug-containing ECM medium was added post-attachment. At 0 h, 24 h, 48 h, 72 h, and 96 h, 100 μL of CCK-8 solution was added per well, followed by incubation at 37 °C for 2 hours. The OD at 450 nm was determined, and growth curves under different drug treatments were plotted.

2.6 EdU Cell Proliferation Assay

TIE2-NC, TIE2-WT, and TIE2-L914F cells were plated in a 48-well plate at a density of 3 × 10^4 cells per well. When cell confluence reached 60%, 200 μL of prepared EdU medium was added according to the instructions of the EdU Cell Proliferation Kit (Ribobio, C10310-1,

Guangzhou, Guangdong, China). After 24 hours of standard culture, cells were fixed and stained with Apollo. Finally, DNA staining was carried out with Hoechst 33342 reaction solution. To investigate the effects of drugs on cell proliferation, cells were treated with drugs for 48 hours, and the medium was removed prior to staining according to the EdU kit instructions. All images were acquired with a fluorescence microscope, and the number of EdU-positive cells was quantified with ImageJ software (National Institutes of Health, Bethesda, MD, USA).

2.7 Apoptosis Detection by Flow Cytometry

TIE2-NC, TIE2-WT, and TIE2-L914F cells were plated in a six-well plate at a density of 3×10^5 cells per well. According to the instructions of the AnnexinV-PE/7-AAD Apoptosis Detection Kit (Meilunbio, Dalian, Liaoning, China), 5 µL of AnnexinV-PE and 5 µL of 7-AAD were supplemented, and the cells were gently mixed and incubated at room temperature in the dark for 15 minutes. To investigate the effects of drugs on apoptosis, cells were treated with drugs for 48 hours, and the medium was discarded before following the kit instructions. Analysis was conducted with a FACSCalibur2 flow cytometer, and data were analyzed using NovoExpress software (Novogene Corporation, Beijing, China).

2.8 Tube Formation Assay

TIE2-NC, TIE2-WT, and TIE2-L914F cells were plated in a 96-well plate pre-coated with 50 µL of Matrigel (Corning, CLS356234, Corning, New York ,USA) at a density of 2×10^4 cells per well and cultured in a 37 °C, 5% CO_2 incubator. To investigate the effects of drugs on angiogenesis, cells were treated with drugs for 48 hours prior to the assay. After seeding, tube formation was monitored at 2-hour intervals and photographed using a fluorescence microscope. The number of vascular junctions and loops was analyzed with ImageJ software (National Institutes of Health, Bethesda, MD, USA).

2.9 Western Blot Analysis

Following Phosphate Buffered Saline (PBS) washing, cells were lysed using Rapamycin lysis buffer containing protease and phosphatase inhibitors for protein extraction. The extracted cellular proteins were subjected to Western blot analysis with the following antibodies: β-Actin (4970, 1:1000, CST, Danvers, Massachusetts, USA), TIE2 (ab221154, 1:1000, Abcam, Cambridge, Cambridgeshire, UK), p-TIE2 (Y992) (ab151704, 1:1000, Abcam, Cambridge, Cambridgeshire, UK), AKT (4691S, 1:1000, CST, Danvers, Massachusetts, USA), p-AKT (Thr308) (13038, 1:1000, CST, Danvers, Massachusetts, USA), p-AKT (Ser473) (4060S, 1:1000, CST, Danvers, Massachusetts, USA), mTOR (2983S, 1:1000, CST, Danvers, Massachusetts, USA), p-mTOR (Ser2448) (5536S, 1:1000, CST, Danvers, Massachusetts, USA), Bcl-2 (ab182858, 1:2000, Abcam, Cambridge , Cambridgeshire, UK), Bcl-2-associated X protein (BAX) (R380709, 1:1000, ZENbio, Chengdu, Sichuan, China), Caspase-3 (341034, 1:1000, ZENbio, Chengdu, Sichuan, China), Cleaved Caspase-3 (ab32042, 1:500, Abcam, Cambridge, Cambridgeshire, UK), P53 (ab32049, 1:1000, Abcam, Cambridge, Cambridgeshire, UK), and Goat Anti-Rabbit IgG H&L (HRP) (ab6721, 1:5000, Abcam, Cambridge, Cambridgeshire, UK). The relative protein expression levels were analyzed with ImageJ software (National Institutes of Health, Bethesda, MD, USA).

2.10 Immunofluorescence

HUVECs in the logarithmic growth phase were plated in a culture plate, and fixation and blocking were carried out when cell confluence reached 80%. The primary antibody, Von Willebrand Factor (ab6994, 1:250, Abcam, Cambridge , Cambridgeshire, UK), was applied overnight at 4 °C. Subsequently, the secondary antibody, Cy3-conjugated goat anti-rabbit IgG (GB21303, Servicebio, 1:250, Wuhan, HuBei, China), was added at 37 °C in the dark for 1 hour, followed by washing. Next, 4′,6-Diamidino-2-phenylindole (DAPI) staining solution (G1012, Servicebio, Wuhan, HuBei, China) was applied in the dark for 10 minutes, followed by another wash. For paraffin-embedded tissue sections, following standard blocking procedures, the primary antibodies CD31 (ab9498, 1:250, Abcam, Cambridge, Cambridgeshire, UK) and p-AKT (Thr308) (ab38449, 1:250, Abcam, Cambridge, Cambridgeshire, UK) were applied overnight at 4 °C. The secondary antibodies, Cy3-conjugated goat anti-mouse IgG (GB21301, 1:250, Servicebio, Wuhan, HuBei, China) and FITC-conjugated goat anti-rabbit IgG (GB22303, 1:250, Servicebio, Wuhan, HuBei, China), were used for CD31 and p-AKT (Thr308), respectively, and were applied at 37 °C in the dark for 1 hour, followed by thorough washing. Finally, DAPI staining solution (G1012, Servicebio, Wuhan, HuBei, China) was applied in the dark for 10 minutes, and after washing, the sections were mounted with resin. All images were acquired with a Nikon microscope system, and the relative protein expression levels were analyzed with ImageJ software (National Institutes of Health, Bethesda, MD, USA).

2.11 Immunohistochemistry

p-AKT (Thr308) Paraffin-embedded tissue sections were incubated with the following primary antibodies: p-TIE2 (Y992) (ab321883, 1:250, Abcam, Cambridge, Cambridgeshire, UK), p-AKT (Thr308) (ab38449, 1:250, Abcam, Cambridge, Cambridgeshire, UK), p-AKT (Ser473) (ab81283, 1:250, Abcam, Cambridge, Cambridgeshire, UK), p-mTOR (Ser2448) (ab109268, 1:250, Abcam, Cambridge, Cambridgeshire, UK), and p53 (ab32049, 1:250, Abcam, Cambridge , Cambridgeshire, UK). Subsequently, the secondary antibody, Goat Anti-Rabbit IgG H&L (HRP) (ab6721, 1:5000, Abcam, Cambridge, Cambridgeshire,

UK), was applied to detect the primary antibodies, and color development was carried out with DAB reagent (DAB-0031, Maixin, Fuzhou, Fujian, China). The sections were stained with hematoxylin for counterstaining. All images were acquired with a Nikon microscope system, and the relative protein expression levels were analyzed with ImageJ software (National Institutes of Health, Bethesda, MD, USA).

2.12 Transcriptome Data Analysis

The transcriptome sequencing dataset GSE130807, comprising venous malformation tissues, was retrieved from the Gene Expression Omnibus (GEO) database, including 5 venous malformation samples and 6 normal venous samples. Differential expression analysis was conducted using the DESeq2 package in RStudio, with the criteria for identifying DEGs set as $|\log2FC| \geq 1$ and adj.p.value < 0.05. The analysis revealed 310 DEGs, which were annotated and visualized. Kyoto Encyclopedia of Genes and Genomes (KEGG) enrichment analysis was performed using the clusterProfiler package, and the results were ranked by gene ratio. Additionally, Gene Set Enrichment Analysis (GSEA) was carried out by ranking genes based on log2FC in descending order to identify enriched pathways, using the human hallmark gene sets from the MSigDB database. GSEA was performed with default parameters ($p$valueCutoff = 0.2), and the results were visualized using the enrichplot package. Furthermore, transcriptome sequencing was performed on TIE2-L914F cells treated with drugs for 48 hours. The dataset was uploaded to the GEO database under the accession number GSE291682, which included 6 samples: 3 samples of TIE2-L914F cells treated with a combination of Rapamycin and Alpelisib for 48 hours, and 3 samples treated with DMSO for 48 hours. Differential expression analysis was performed using the DESeq2 package, with the criteria for identifying DEGs set as $|\log2FC| \geq 0.378$ and adj.p.value < 0.05. The analysis identified 439 DEGs, which were annotated and visualized. KEGG pathway enrichment analysis was conducted using the clusterProfiler package, and the results were ranked by gene ratio. GSEA was also performed by ranking genes based on log2FC in descending order, using the human hallmark gene sets from the MSigDB database. GSEA was performed with default parameters ($p$valueCutoff = 0.2), and the results were visualized using the enrichplot package.

2.13 3D Tubule Formation Assay

The fibrin bead assay was previously described in detail [23]. In this study, Cytodex® 3 microcarrier beads (Sigma, Louis, Missouri, USA) were coated with TIE2-L914F cells at 1500 cells per bead and embedded in fibrin gel. Fibroblasts (Cells are identified by surface marker analysis by flow cytometry, **Supplementary Fig. 1D**) were seeded onto the gel surface, and the ECM medium was refreshed every 2 days. On day 0, the designated drugs were added to the wells. After 2 days of treatment, the drugs were removed, and fresh medium was added. On day 7, the fibroblast layer overlaying the fibrin gel was removed by trypsin treatment. Images were acquired using a Nikon microscope, and the number of vascular sprouts per bead was quantified by two independent blinded observers.

2.14 Venous Malformation Xenograft Model in Nude Mice

The nude mice (nu/nu, Kunming Medical University Animal Research Institute, China) used in this study were purchased from the Kunming Medical University Animal Research Institute. First, TIE2-L914F cells were pretreated with drugs or DMSO for 48 hours. Then, 2.5×10^6 cells were collected and suspended in 200 µL of Matrigel® (Corning, CLS356234, Corning, New York, USA). The cell suspension was subcutaneously injected into both sides of the dorsal region of 4- to 6-week-old male nude mice. Drug-treated cells were injected on one side (experimental group), while DMSO-treated cells were injected on the other side (control group), with an equal number of cells injected on each side. After 14 days, the nude mice were anesthetized by intraperitoneal injection of sodium pentobarbital (10 mg/mL) at a dose of 40–50 mg/kg, followed by euthanasia via cervical dislocation under anesthesia. Tumors at the injection sites were excised, weighed, and fixed in 4% paraformaldehyde solution, followed by paraffin embedding. Sections of 5 µm thickness were cut for immunofluorescence (IF) and immunohistochemical (IHC) staining. Images were captured using a Nikon microscope, and the vascular area and target protein average optical density (AOD) values were quantitatively analyzed using ImageJ software (National Institutes of Health, Bethesda, MD, USA).

2.15 Data Analysis

Data are presented as mean ± standard error of the mean (SEM). Welch's t-test or parametric one-way analysis of variance (ANOVA) was applied after confirming normality and homogeneity of variance. Multiple comparisons were conducted with Tukey's or Fisher's post hoc tests after one-way ANOVA. For repeated measures data, two-way ANOVA was applied, followed by Bonferroni post hoc tests. All calculations were conducted with GraphPad Prism 10.0 software (GraphPad Software, San Diego, CA, USA), and $p < 0.05$ was considered statistically significant.

3. Results

3.1 The Main Pathological Features of VMs Include Abnormal Angiogenesis and Hyperactivation of the PI3K Pathway

The heatmap revealed 310 significantly dysregulated genes in VMs tissues compared to normal tissues (Fig. 1A). KEGG pathway analysis demonstrated that the PI3K-AKT signaling pathway was significantly enriched in the disease group and ranked as the top enriched path-

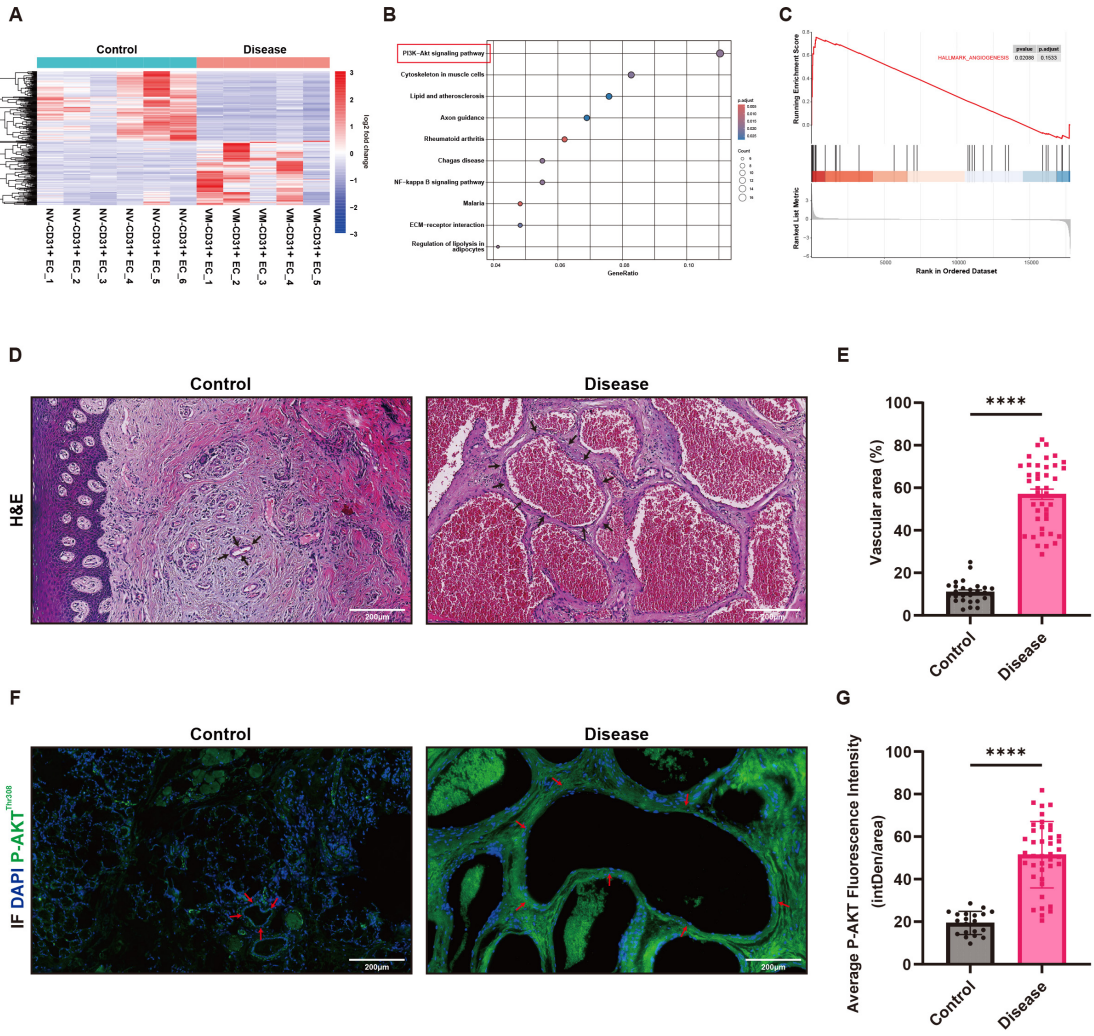

Fig. 1. Overactivation of the Phosphoinositide 3-Kinase/Protein Kinase B (PI3K-AKT) pathway and abnormal angiogenesis in venous malformation (VM) tissues. (A) Heatmap depicting the expression profiles of 310 differentially expressed genes in VM tissues (Disease, n = 5) and normal tissues (Control, n = 6). Red represents high expression, and blue represents low expression. (B) Kyoto Encyclopedia of Genes and Genomes (KEGG) pathway analysis reveals that the PI3K-AKT signaling pathway is significantly enriched and ranked first in the disease group. (C) Gene Set Enrichment Analysis (GSEA) analysis demonstrates that the biological process of angiogenesis (HALLMARK_ANGIOGENESIS) is exhibit marked biological enrichment tendency in the disease group (p = 0.02088, p.adjust = 0.1533). (D) H&E staining reveals significant dilation of vascular lumens in VM tissues, with clear differences compared to normal skin and gingival tissues (VM tissues n = 41, normal tissues n = 21, Scale bar = 200 μm). (E) Quantitative analysis reveals that the vascular area in the disease group is significantly higher than in the normal group (mean ± SEM, ****$p < 0.0001$). (F) Immunofluorescence staining reveals significantly elevated p-AKT expression in the disease group. Green indicates p-AKT signal, and blue indicates 4′,6-Diamidino-2-phenylindole (DAPI)-stained nuclei (VM tissues n = 41, normal tissues n = 20, Scale bar = 200 μm). (G) Quantitative analysis reveals that the fluorescence intensity of p-AKT in the disease group is significantly higher than in the normal group (mean ± SEM, ****$p < 0.0001$).

way (Fig. 1B). Additionally, pathways associated with cytoskeleton regulation and extracellular matrix interactions were also significantly enriched in the disease group (Fig. 1B). Further GSEA analysis indicated significant enrichment of the angiogenesis biological process (HALLMARK_ANGIOGENESIS, Fig. 1C), with a nominal p-value of 0.02088. However, the adjusted p-value (p.adjust = 0.1533) did not reach statistical significance, potentially due to the limited sample size or the gene ranking approach.

HE and immunofluorescence staining of VMs tissue sections demonstrated a significantly increased vascular area in VMs tissues compared to normal skin or gingival tissues (Fig. 1D,E), suggesting marked abnormal angiogenesis in the disease group. Furthermore, the expression of

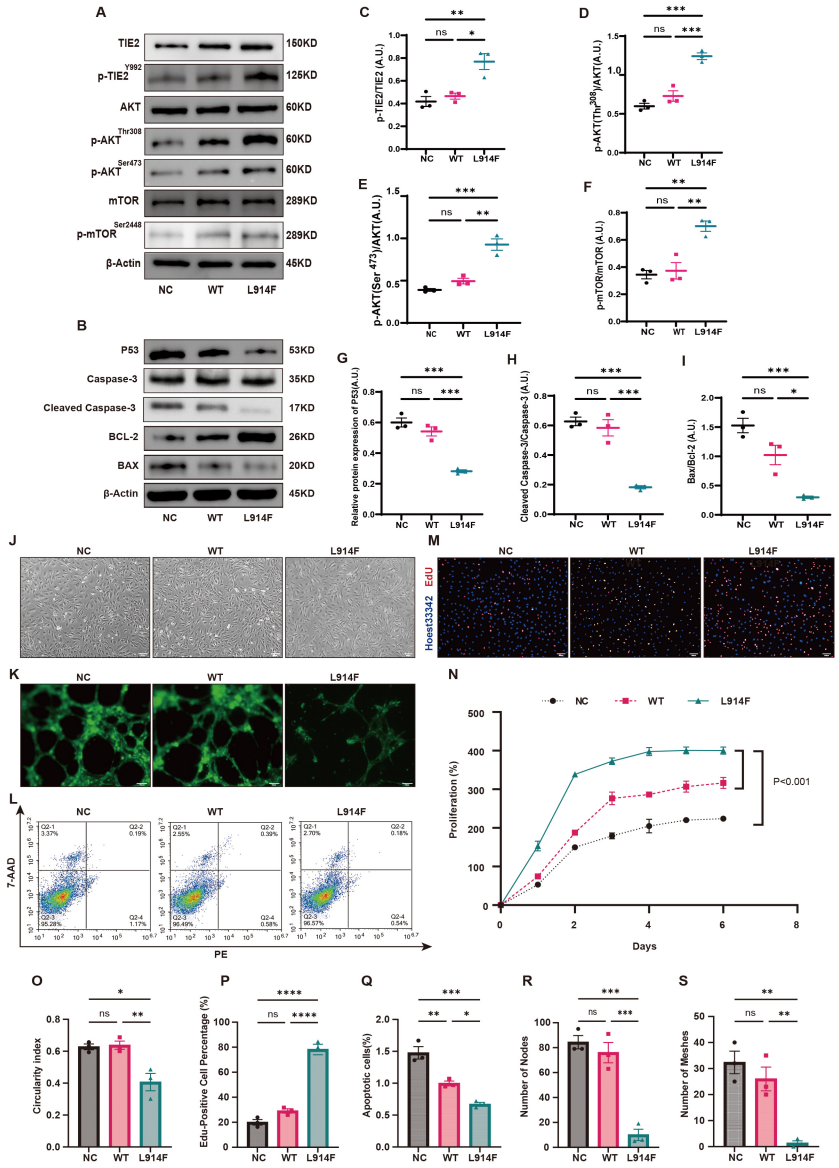

Fig. 2. The TIE2 p.Leu914Phe (TIE2-L914F) mutation alters the phenotype of normal cells and related signaling pathways. (A) Western blot reveals that the expression of p-TIE2, p-AKT (Thr308 and Ser473), and p-mTOR in the TIE2-L914F mutation group (L914F) is significantly higher than in the control group (NC) and wild-type group (WT) (n = 3). (B) Western blot reveals that the expression of P53, Cleaved Caspase-3, and Bcl-2-associated X protein (BAX) is significantly reduced in the L914F mutation group (n = 3). (C–F) Quantitative analysis reveals that p-TIE2/TIE2 (C), p-AKT (Thr308)/AKT (D), p-AKT (Ser473)/AKT (E), and p-mTOR/mTOR (F) in the L914F mutation group are significantly higher than in the NC and WT groups (mean ± SEM, ns indicates no significant statistical difference, *$p < 0.05$, **$p < 0.01$, ***$p < 0.001$). (G–I) Quantitative analysis reveals that the expression of P53 (G), Cleaved Caspase-3 (H), and Bcl-2-associated X protein(BAX) (I) in the L914F mutation group is significantly reduced (mean ± SEM, ns indicates no significant statistical difference, *$p < 0.05$, ***$p < 0.001$). (J) Under inverted microscopy, L914F cells exhibited elongated/spindle-like morphology and reduced roundness (n = 3), Scale bar = 200 μm. (K) Tubule formation assay reveals that the angiogenesis ability of the L914F mutation group is significantly reduced, with fewer nodes and tubular structures (n = 3), Scale bar = 200 μm. (L) Flow cytometry reveals that the apoptosis rate in the L914F mutation group is significantly lower than in the NC and WT groups (n = 3). (M) EdU assay reveals that the proliferation ability of the L914F mutation group is significantly enhanced, with a higher proportion of EdU-positive cells compared to the NC and WT groups (red: EdU-positive cells, blue: Hoechst-stained nuclei, n = 3), Scale bar = 50 μm. (N) Cell proliferation curve reveals that the proliferation rate of the L914F mutation group is significantly higher than in the NC and WT groups (mean ± SEM, $p < 0.001$, n = 3). (O–S) Quantitative analysis reveals that the L914F mutation group exhibits reduced cell roundness (O), increased proportion of EdU-positive cells (P), decreased apoptosis rate (Q), and reduced numbers of vascular nodes (R) and network structures (S) (mean ± SEM, ns indicates no significant statistical difference, *$p < 0.05$, **$p < 0.01$, ***$p < 0.001$, ****$p < 0.0001$).

p-AKT protein was significantly elevated in VMs tissues compared to normal tissues (Fig. 1F,G), further supporting the hyperactivation of the PI3K pathway in VMs.

3.2 TIE2-L914F Mutant HUVECs: PI3K Activation, P53 Downregulation and Phenotypic Alterations

HUVECs were transduced via lentiviral-mediated gene delivery with a TIE2-L914F mutant construct, successfully establishing a TIE2-L914F mutant VM cell model and providing a solid experimental foundation for subsequent mechanistic studies. Initially, Western blot analysis was performed to assess the impact of the TIE2-L914F mutation on the PI3K signaling pathway (Fig. 2A). Analysis revealed that the expression of p-TIE2 was significantly elevated in the TIE2-L914F mutation group (L914F) compared to the control (NC) and wild-type TIE2 (WT) groups (Fig. 2C). Additionally, downstream signaling molecules, including p-AKT (p-AKT Thr308 and Ser473, Fig. 2D,E) and p-mTOR (Fig. 2F), were also significantly upregulated, indicating hyperactivation of the PI3K pathway in cells with the TIE2-L914F mutation. Analysis of apoptosis-related markers (Fig. 2B) demonstrated that p53 expression was significantly downregulated in the L914F group (Fig. 2G), along with reduced levels of Cleaved Caspase-3 (Fig. 2H) and the pro-apoptotic protein BAX (Fig. 2I), suggesting that the TIE2-L914F mutation inhibits apoptosis through p53 downregulation. Additionally, the L914F group exhibited significant morphological changes, with cells displaying elongated or spindle-shaped forms compared to the NC and WT groups (Fig. 2J), accompanied by a reduction in cellular roundness (Fig. 2O). EdU staining revealed that the TIE2-L914F mutation promoted cell proliferation, with the L914F group showing a significantly higher proliferation rate than the NC and WT groups (Fig. 2M,P). The cell proliferation curve further demonstrated accelerated proliferation in the L914F group (Fig. 2N). In the tubule formation assay, the tubule formation capacity in the L914F group was significantly impaired (Fig. 2K), with fewer vascular nodes (Fig. 2R) and ring-like structures (Fig. 2S) compared to controls. Flow cytometry revealed a significantly lower apoptosis rate in the L914F group than in the NC and WT groups (Fig. 2L,Q).

Collectively, the TIE2-L914F mutation upregulates p-TIE2 expression, hyperactivates the PI3K signaling pathway, and suppresses p53 in venous endothelial cells. These findings suggest a pathological mechanism underlying abnormal cell morphology, enhanced proliferation, impaired angiogenesis, and inhibited apoptosis.

3.3 PI3K Targeting Reverses TIE2-L914F Mutant Endothelial Cell Phenotypes: Rapamycin-Alpelisib Synergy

The cell growth curve (**Supplementary Fig. 1E**) revealed that cell proliferation was significantly inhibited after 48 hours of drug treatment compared to controls, prompting the standardization of a 48-hour treatment period for subsequent experiments. Western blot analysis demonstrated that PI3K inhibitors, either alone or in combination, effectively suppressed the PI3K pathway (Fig. 3A). Notably, the combination of Rapamycin and Alpelisib exhibited the strongest inhibitory effect, characterized by significantly reduced expression of p-TIE2 (Fig. 3C), p-AKT (Thr308 and Ser473, Fig. 3D,E), and p-mTOR (Fig. 3F). Compared to single-agent treatments or the recommended combination (Rapamycin + Ponatinib), Rapamycin and Alpelisib showed enhanced synergistic effects, suggesting promising therapeutic potential against PI3K pathway hyperactivation. Analysis of apoptosis-related markers (Fig. 3B) revealed that the Rapamycin and Alpelisib combination significantly upregulated p53 expression (Fig. 3G) and increased levels of pro-apoptotic proteins Cleaved Caspase-3 (Fig. 3H) and BAX (Fig. 3I), further supporting its potent pro-apoptotic effects compared to other treatments. Functional assays confirmed the reversal of TIE2-L914F pathological phenotypes upon PI3K pathway inhibition. The Rapamycin and Alpelisib combination significantly improved cell morphology (Fig. 3J), increased cellular roundness (Fig. 3N), suppressed abnormal proliferation (Fig. 3K,O), and enhanced apoptosis (Fig. 3L,P). Tubule formation assays demonstrated that this combination restored normal angiogenesis (Fig. 3M), characterized by increased vascular nodes (Fig. 3Q) and ring-like structures (Fig. 3R), indicating superior therapeutic effects compared to single agents or the recommended combination.

Collectively, the Rapamycin and Alpelisib combination synergistically inhibits the PI3K pathway, effectively reversing pathological phenotypes in TIE2-L914F mutant endothelial cells and demonstrating significant therapeutic potential.

3.4 Rapamycin and Alpelisib Combination Exhibits High Safety and Target Specificity

Regarding cell morphology, the Rapamycin and Alpelisib combination significantly reversed morphological abnormalities in TIE2-L914F mutant cells while exerting minimal effects on control (NC) and wild-type (WT) groups (Fig. 4A). Notably, cellular roundness was significantly increased in TIE2-L914F mutant cells (Fig. 4F), with no significant changes in NC and WT groups. Regarding cell proliferation, the combination significantly inhibited abnormal proliferation in TIE2-L914F mutant cells (Fig. 4B,C), showing significantly greater proliferation inhibition compared to NC and WT groups (Fig. 4G). Flow cytometry revealed that the combination significantly promoted apoptosis in TIE2-L914F mutant cells (Fig. 4D), exhibiting a significantly increased apoptosis rate compared to NC and WT groups (Fig. 4H). Regarding angiogenesis, the combination restored normal angiogenesis in TIE2-L914F mutant cells (Fig. 4E), significantly enhancing vascular node (Fig. 4J) and network structure formation (Fig. 4I),

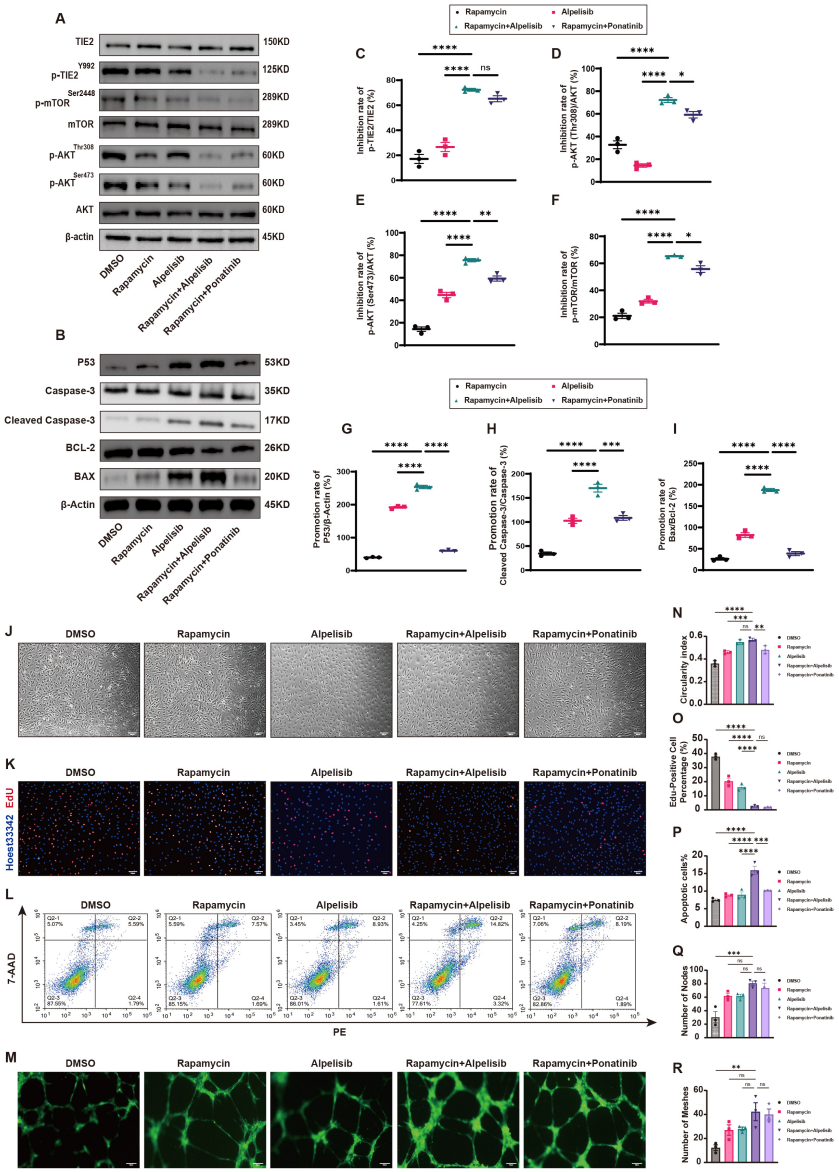

Fig. 3. Rapamycin and Alpelisib combination ameliorates TIE2-L914F pathological features via PI3K/AKT/mTOR inhibition and p53 restoration. (A) Western blot reveals that PI3K inhibitors significantly suppress the activation of the PI3K/AKT/mTOR pathway (n = 3). (B) Western blot reveals that PI3K inhibitors significantly upregulate the expression of P53, Cleaved Caspase-3, and BAX proteins (n = 3). (C–F) Quantitative analysis reveals that the Rapamycin and Alpelisib combination significantly inhibits the expression of p-TIE2/TIE2 (C), p-AKT (Thr308)/AKT (D), p-AKT (Ser473)/AKT (E), and p-mTOR/mTOR (F) (mean ± SEM, ns indicates no significant statistical difference, *$p < 0.05$, **$p < 0.01$, ****$p < 0.0001$). (G–I) Quantitative analysis reveals that the combination significantly upregulates the expression of P53 (G), Cleaved Caspase-3 (H), and BAX (I) (mean ± SEM, ***$p < 0.001$, ****$p < 0.0001$). (J) Under microscopy, the combination treatment of Rapamycin and Alpelisib significantly rescued the aberrant morphology of TIE2-L914Fmutant cells and increased cellular roundness (n = 3), Scale bar = 200 μm. (K) EdU assay reveals that the combination significantly inhibits the proliferation of mutant cells, with a reduced proportion of EdU-positive cells (red: EdU-positive cells, blue: Hoechst-stained nuclei, n = 3), Scale bar = 200 μm. (L) Flow cytometry reveals that the combination significantly enhances apoptosis in mutant cells, with an increased proportion of apoptotic cells (n = 3). (M) Tubule formation assay reveals that the combination significantly restores angiogenesis in mutant cells, increasing vascular nodes and network structures (n = 3), Scale bar = 50 μm. (N–R) Quantitative analysis reveals that the combination significantly improves cell roundness (N), reduces EdU-positive cells (O), increases apoptotic cells (P), and enhances vascular nodes (Q) and network structures (R) (mean ± SEM, ns indicates no significant statistical difference, **$p < 0.01$, ***$p < 0.001$, ****$p < 0.0001$).

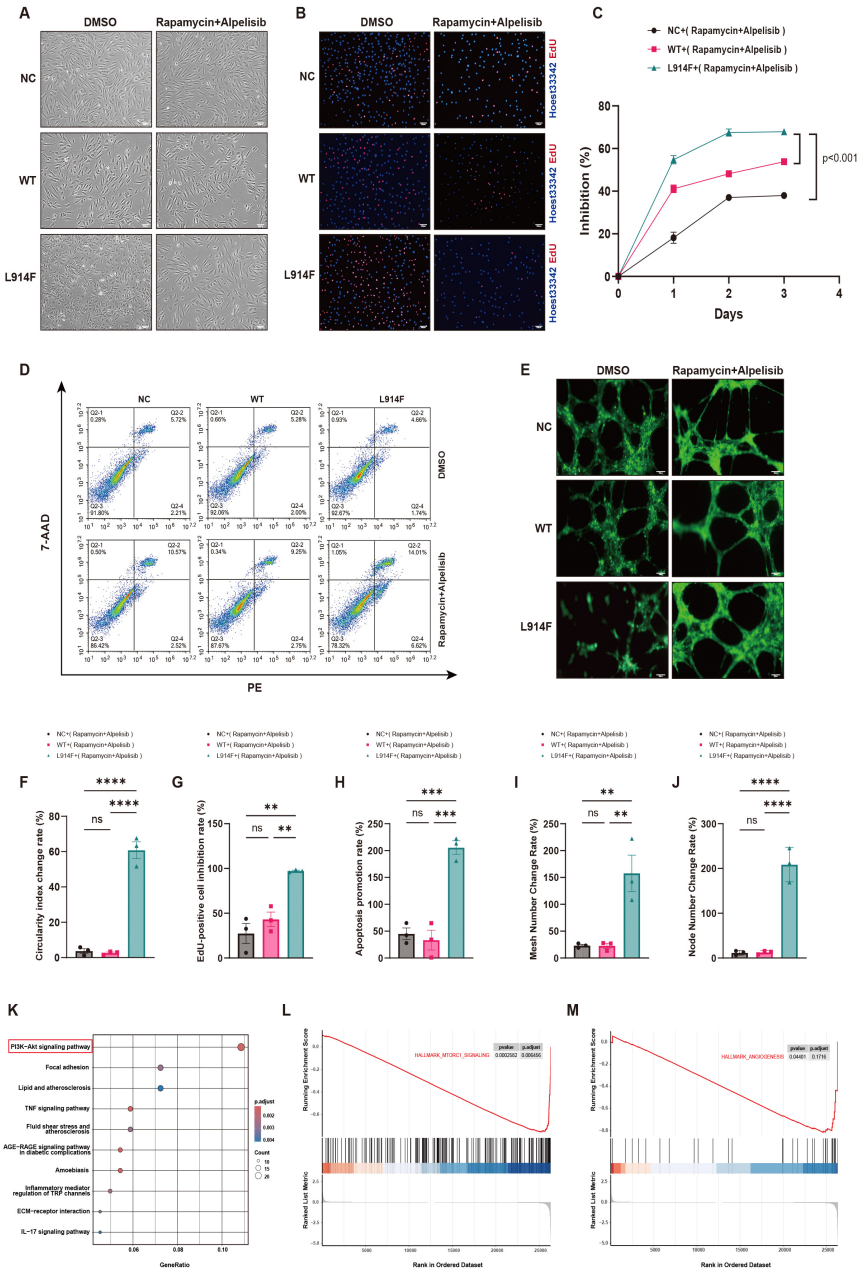

Fig. 4. Rapamycin and Alpelisib combination exhibits high safety and target specificity. (A) Inverted microscopy reveals that the combination significantly improves the abnormal morphology of TIE2-L914F mutant cells but has no significant effect on the morphology of normal control (NC) and wild-type (WT) cells (n = 3), Scale bar = 200 μm. (B) EdU assay reveals that the combination significantly inhibits the proliferation of TIE2-L914F mutant cells but has minimal effects on NC and WT cells (red: EdU-positive cells, blue: Hoechst-stained nuclei, n = 3), Scale bar = 200 μm. (C) Cell proliferation curve reveals that the combination significantly inhibits the proliferation of mutant cells but has minimal effects on NC and WT groups (mean ± SEM, $p < 0.001$, n = 3). (D) Flow cytometry reveals that the combination significantly enhances the apoptosis rate of mutant cells but has minimal effects on NC and WT groups (n = 3). (E) Tubule formation assay reveals that the combination restores angiogenesis in mutant cells but does not significantly affect NC and WT groups (n = 3), Scale bar = 50 μm. (F–J) Quantitative analysis reveals that the combination significantly improves the roundness of TIE2-L914F mutant cells (F), reduces EdU-positive cells (G), increases apoptosis rate (H), and network structures (I) and enhances vascular nodes (J), with no significant effects on NC and WT groups (mean ± SEM, ns indicates no significant statistical difference, $^{**}p < 0.01$, $^{***}p < 0.001$, $^{****}p < 0.0001$). (K) KEGG pathway analysis reveals that the PI3K-AKT signaling pathway is significantly enriched and ranked first in the combination treatment model, indicating its role as the core pathway of drug action. (L,M) GSEA analysis reveals that the combination significantly suppresses the mTORC1 signaling pathway (L, HALLMARK_MTORC1_SIGNALING) and angiogenesis (M, HALLMARK_ANGIOGENESIS), further validating its target specificity.

while exerting no significant effects on NC and WT groups. These results demonstrate that the Rapamycin and Alpelisib combination exhibits high selectivity and safety, exerting minimal effects on normal cells but significant therapeutic effects on TIE2-L914F mutant cells. Subsequently, transcriptome sequencing was performed on TIE2-L914F mutant cells treated with the Rapamycin and Alpelisib combination to further explore the underlying mechanisms. KEGG pathway analysis revealed that the PI3K-AKT signaling pathway was significantly enriched and ranked first (Fig. 4K), indicating that the combination primarily targets this pathway. GSEA further confirmed that the combination significantly inhibited the MTORC1 signaling pathway (HALLMARK_MTORC1_SIGNALING, Fig. 4L) and angiogenesis (HALLMARK_ANGIOGENESIS, Fig. 4M), validating the target specificity of this combination therapy against disease mechanisms and phenotypes.

Collectively, within 48 hours, the low-concentration combination of Rapamycin and Alpelisib exhibits high selectivity and target specificity against the TIE2-mutated venous malformation cell model, while exerting minimal effects on normal endothelial cells. By targeting the PI3K pathway, it effectively inhibits proliferation, promotes apoptosis, and restores normal angiogenesis in TIE2-L914F mutant cells.

3.5 Rapamycin and Alpelisib Combination Suppresses Angiogenesis in 3D Tubule Formation and Lesion Development in Nude Mice

The efficacy of the Rapamycin and Alpelisib combination was further assessed using a 3D angiogenesis assay, as illustrated in Fig. 5A. In the 3D tubule formation assay, the combination significantly suppressed angiogenesis in TIE2-L914F mutant venous endothelial cells. Compared with the control (DMSO) and other treatment groups (Rapamycin, Alpelisib, and Rapamycin + Ponatinib), the Rapamycin and Alpelisib combination significantly decreased vascular branching (Fig. 5B), with quantitative analysis revealing a significant reduction in vascular sprout numbers (Fig. 5C). These results demonstrate that the combination exerts significant anti-angiogenic effects. Next, the efficacy of the combination was evaluated in nude mice, as illustrated in Fig. 5D. Lesions formed by TIE2-L914F mutant venous endothelial cells mixed with Matrigel were significantly suppressed in the Rapamycin and Alpelisib group (Fig. 5E), with lesion weight significantly reduced compared to controls (Fig. 5F). Immunofluorescence and immunohistochemical analysis further demonstrated that the combination significantly reduced the vascular area in lesion tissues (Fig. 5G,M), indicating effective suppression of lesion formation. Additionally, the combination significantly decreased the expression of p-TIE2 (Fig. 5H,N), p-AKT (Thr308 and Ser473, Fig. 5I,J,O,P), and p-mTOR (Fig. 5K,Q) in lesion tissues, while significantly increasing p53 expression (Fig. 5L,R). These findings indicate that the combination effectively suppresses lesion progression by targeting the PI3K/AKT/mTOR pathway and regulating p53 signaling.

Collectively, the Rapamycin and Alpelisib combination significantly inhibits angiogenesis in 3D assays and suppresses lesion formation in nude mice. Through precise targeting of the PI3K/AKT/mTOR pathway and regulation of p53 expression, this combination therapy provides critical experimental evidence for treating TIE2-L914F mutation-related VMs.

4. Discussion

4.1 Preliminary Investigation into the Role and Pathological Mechanisms of the PI3K Pathway in TIE2-Mutant Venous Malformations

Dysfunction of the PI3K pathway is prevalent in various VMs and represents one of the key molecular pathological mechanisms [12]. Although the PI3K pathway has been extensively studied in VMs associated with PIK3CA activating mutations [13,15,16], its role in VMs caused by TIE2 activating mutations remains poorly understood [24]. This study provides important experimental data on the role of the PI3K pathway in VMs with TIE2 activating mutations and provides a theoretical foundation for further targeted therapeutic strategies.

Initially, we compared the gene expression profiles of VM tissues and normal venous tissues through transcriptome sequencing analysis. The significant enrichment of the PI3K-AKT signaling pathway further supported the critical role of this pathway in the pathogenesis of VMs. The significant enrichment of pathways related to cytoskeleton regulation and extracellular matrix interactions further suggested that VMs may be associated with abnormal cell morphology and structure. Additionally, the significant activation of angiogenesis highlighted its critical role in the pathological process of VMs, consistent with the clinically observed characteristics of abnormal vascular proliferation [25]. To validate these findings, we performed HE and immunofluorescence staining on VM tissue sections, further supporting that the main pathological features of the disease are abnormal angiogenesis and overactivation of the PI3K pathway, providing important clues for further research into its pathogenic mechanisms.

4.2 Regulatory Effects of TIE2-L914F Mutation on the PI3K Pathway and Venous Malformation Cell Phenotypes

The TIE2-L914F mutation represents the most frequent pathogenic mutation in sporadic VMs [18]. Although the PI3K pathway has been extensively studied in VMs associated with PIK3CA activating mutations, its specific role in VMs caused by TIE2-L914F mutations remains elusive. Therefore, we constructed a VM cell model with the TIE2-L914F mutation using lentiviral technology and demonstrated that the TIE2-L914F mutation hyperactivates the PI3K pathway by activating p-TIE2. This led to elongated

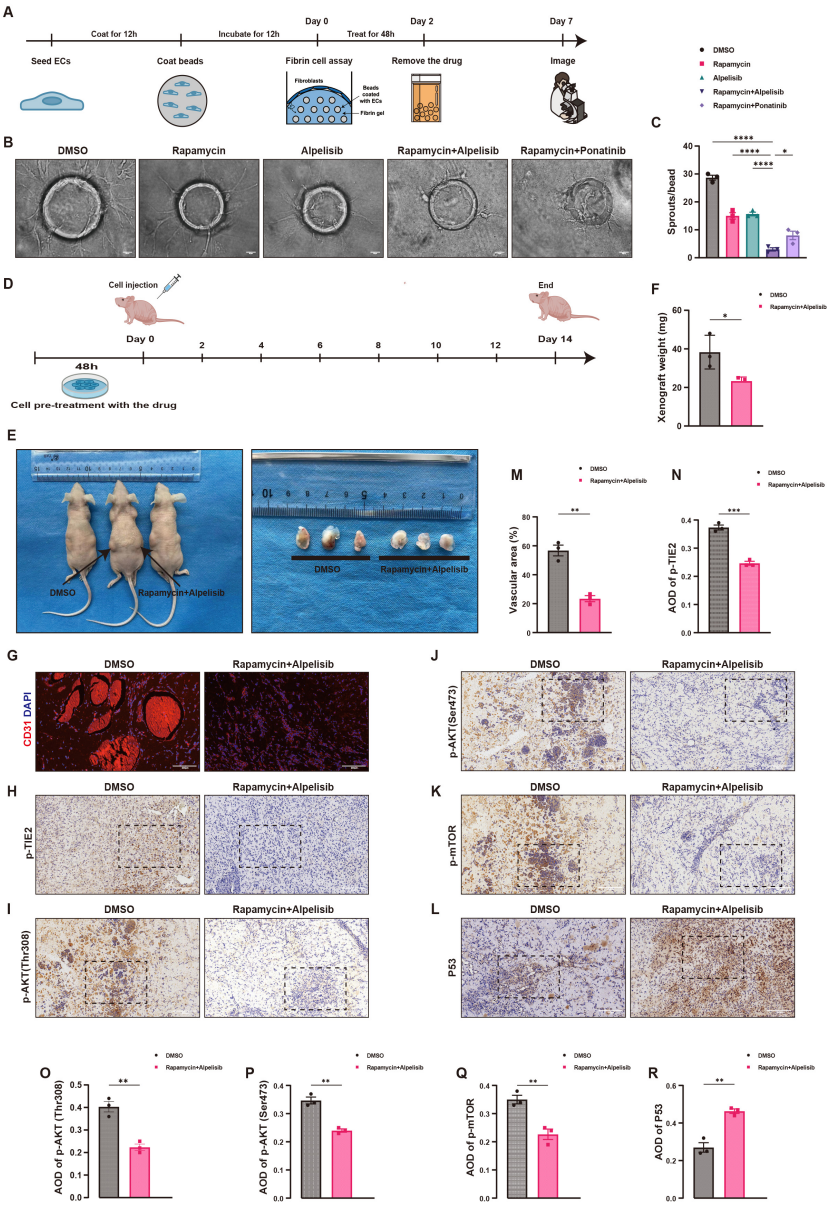

Fig. 5. Rapamycin and Alpelisib combination suppresses angiogenesis in 3D tubule formation and lesion development in nude mice. (A) Flowchart of the 3D tubule formation assay, illustrating the timeline of fibrin gel embedding, drug treatment, and tubule formation analysis. (B) 3D tubule formation assay images reveal that the Rapamycin and Alpelisib combination significantly inhibits vascular sprout formation compared to the Dimethyl Sulfoxide (DMSO) control and other drug groups (n = 3), Scale bar = 50 μm. (C) Quantitative analysis reveals that the number of vascular sprouts in the Rapamycin and Alpelisib group is significantly lower than in the DMSO control and other drug groups (mean ± SEM, $*p < 0.05$, $****p < 0.0001$). (D) Flowchart of the nude mouse xenograft model experiment, illustrating the timeline of cell pretreatment, injection, and analysis. (E) Representative macroscopic images of lesion tissues from the Rapamycin and Alpelisib group and the DMSO control group. (F) Quantitative analysis reveals that the Rapamycin and Alpelisib combination significantly reduces lesion weight in nude mice compared to the DMSO control group (mean ± SEM, $*p < 0.05$). (G) Immunofluorescence staining showed that, compared with the dimethyl sulfoxide (DMSO) control group, the combination treatment of Rapamycin and Alpelisib significantly reduced the vascular area in the lesion tissues. (H–L) Immunohistochemical (IHC) analysis revealed that, compared with the DMSO control group, the combination of Rapamycin and Alpelisib significantly inhibited the expression levels of phosphorylated TIE2 (H), phosphorylated AKT at threonine 308 (I), phosphorylated AKT at serine 473 (J), and phosphorylated mTOR (K), while significantly upregulating the expression of p53 (L) (n = 3), Scale bar = 200 μm. (M–R) Quantitative analysis further demonstrates that the combination significantly reduces the vascular area (M), p-TIE2 (N), p-AKT (Thr308) (O), p-AKT (Ser473) (P), and p-mTOR (Q) expression levels in lesion tissues, while significantly increasing p53 (R) expression (mean ± SEM, $**p < 0.01$, $***p < 0.001$).

or spindle-shaped changes in endothelial cell morphology, promoted cell proliferation, downregulated p53 to inhibit apoptosis, and impaired normal angiogenesis, driving lesion development. This cellular phenotype further supports the fundamental nature of venous malformations as congenital developmental vascular anomalies, which are non-neoplastic lesions, and in which abnormal endothelial cell proliferation constitutes one of their core histopathological features [26,27]. The genetic basis of VMs involves acquired pathogenic mutations that lead to overactivation of the PI3K pathway, thereby triggering the disease. Therefore, therapeutic strategies targeting the PI3K pathway hold significant promise in the treatment of VMs [28–30].

4.3 The Synergistic Therapeutic Effects of Rapamycin-Alpelisib Combination In Vitro and In Vivo

Current research has shown that Rapamycin has been used in clinical trials, but as a monotherapy, it has certain limitations in therapeutic efficacy [31,32]. Alpelisib is a selective PI3Kα (p110α) inhibitor, which has demonstrated significant efficacy in the treatment of PIK3CA-related overgrowth spectrum (PROS) and vascular malformations (VMs). It has emerged as a new targeted therapeutic strategy, attracting widespread attention in the clinical community. Compared with Rapamycin, Alpelisib can act directly on the upstream of the PI3K signaling pathway, with more precise targeting specificity, thus potentially achieving more prominent clinical effects [33]. In 2022, the US Food and Drug Administration (FDA) approved Alpelisib for the treatment of pulmonary arterial hypertension in patients aged 2 years and older. Ongoing clinical trials, including EPIK-P2, are actively evaluating its application potential in a broader range of vascular abnormalities. Although adverse events, including hyperglycemia and diarrhea, have been observed in some patients, the treatment was overall well-tolerated, suggesting that Alpelisib holds great potential as a precision therapeutic approach for severe VMs and related vascular anomalies [34]. To elucidate the role of the PI3K pathway in TIE2-L914F mutations and evaluate the effects of targeted therapy, this study selected several commonly used PI3K inhibitors for investigation. The inhibitor concentrations were determined based on previous literature and preliminary screening [21,22]. To evaluate potential synergy and the therapeutic effects of the combination, the dose of the combination therapy was set to half of the experimental concentration of each single drug. This experimental design is based on the hypothesis that the two drugs may exhibit synergistic effects at low doses, which can not only achieve significant therapeutic effects but also potentially reduce toxicity to endothelial cells within 48 hours. Additionally, this dose setting allows for a better evaluation of whether the combination has synergistic or additive effects, providing a basis for subsequent dose optimization and clinical application.

Unexpectedly, we observed that the combination of Rapamycin and Alpelisib significantly inhibited the abnormal activation of the PI3K/AKT/mTOR pathway. This combination restored p53 signaling, significantly inhibited the proliferation of mutant cells, promoted apoptosis, and restored angiogenesis. Previous studies have shown that Rapamycin in combination with ponatinib, an ABL kinase inhibitor, can induce regression of venous malformations in mice and suppress AKT phosphorylation [22]. Compared with monotherapy or the previously reported combination regimen (Rapamycin + ponatinib), the combined treatment of Rapamycin and Alpelisib exerted significantly stronger synergistic inhibitory effects on cell apoptosis, the PI3K pathway, and the p53 pathway. These findings suggest that this dual-drug combination holds promising therapeutic potential for targeting hyperactivation of the PI3K pathway and inhibition of the p53 pathway, providing an important experimental basis for the clinical translation of this strategy. In our preliminary experiments, we also tested the triple combination of Rapamycin, Alpelisib, and ponatinib in HUVEC-TIE2-L914F cells. However, even at lower drug concentrations, extensive cell death occurred within 24 h of treatment. We hypothesize that this outcome may result from drug–drug interactions among the three agents, leading to enhanced cytotoxicity. Although traditional tubule formation assays provide some insights into angiogenesis, they are limited in simulating the real disease environment *in vivo*. Therefore, we further assessed the efficacy of the Rapamycin and Alpelisib combination using 3D tubule formation assays and a nude mouse xenograft model. The results demonstrated that the combination significantly inhibited 3D angiogenesis and effectively slowed the formation and progression of lesions in nude mice. Mechanistic studies demonstrated that the combination exhibited multi-target synergistic potential by efficiently inhibiting the PI3K/AKT/mTOR pathway and activating p53 signaling.

4.4 Crosstalk Between the PI3K-AKT/mTOR and p53 Pathways and Their Potential Therapeutic Mechanisms

The PI3K-AKT signaling pathway and p53 signaling pathway are key intracellular signal transduction pathways that play a central role in regulating fundamental cellular processes including cell growth, proliferation, apoptosis, and metabolism. In recent years, studies have confirmed that aberrant activation or dysfunction of these two pathways is closely associated with the initiation and progression of various diseases, and there exists intricate subcellular crosstalk between them. Genotoxic stress can induce nuclear AKT activation, a process dependent on p53-mediated regulatory mechanisms, which is significantly distinct from the canonical membrane-localized activation mode of the PI3K-AKT pathway. Specifically, upon genotoxic stress, nuclear PI3K can bind to p53 in the non-membranous nucleoplasm to form a complex of p53 and

phosphatidylinositol 3,4,5-trisphosphate (PtdIns(3,4,5)P3). This complex recruits AKT, Pyruvate Dehydrogenase Kinase 1 (PDK1), and mechanistic target of Rapamycin complex 2 (mTORC2), thereby activating AKT and phosphorylating Forkhead box O1 (FOXO) proteins, ultimately inhibiting DNA damage-induced cell apoptosis [35] (A p53-phosphoinositide signalosome regulates nuclear AKT activation). In the context of venous malformations, researchers have demonstrated that Rapamycin ameliorates the physiological functions of TIE2-mutant endothelial cells by inhibiting the AKT-mTOR pathway; meanwhile, it promotes the nuclear translocation of FOXO1 and the expression of PDGFB in cells, further improving the paracrine interaction between endothelial cells and smooth muscle cells (SMCs). Based on these findings, the AKT-FOXO1 axis has been proposed as a potential therapeutic target for TIE2-mutated venous malformations [36].

In the present study, we found that hyperactivation of the AKT-mTOR signaling pathway and suppression of p53 signaling occurred in TIE2-mutant HUVECs. Notably, combined treatment with Rapamycin and Alpelisib significantly inhibited the aberrant activation of the PI3K/AKT/mTOR pathway and restored p53 signaling expression in these mutant cells. Therefore, we hypothesize that the intricate subcellular crosstalk between the PI3K-AKT and p53 pathways may ameliorate the phenotypic abnormalities of venous malformation endothelial cells and exert potential therapeutic effects via the mechanism of nuclear PI3K binding to p53 to form a complex, which in turn recruits AKT/PDK1/mTORC2, activates AKT, and phosphorylates FOXO proteins. This feedback regulatory mechanism reveals the complex interactive pattern of the two pathways at the level of gene transcription in TIE2-mutated venous malformations. In fact, the PI3K-AKT and p53 signaling pathways exhibit multi-dimensional and tight mutual regulatory relationships: they not only achieve direct molecular crosstalk through mechanisms such as p53-dependent nuclear AKT activation and PI3K-AKT-mediated p53 degradation, but also display widespread co-enrichment characteristics and synergistic regulatory effects in various disease states. We thus speculate that the close association between these two pathways in venous malformations may lead to compensatory activation of one pathway when the other is targeted alone, thereby compromising the therapeutic efficacy. Future studies are warranted to clarify the specific interactive mechanisms of these two pathways in venous malformations through additional experiments, which will provide a theoretical basis for the development of novel targeted therapeutic agents and combination treatment strategies.

5. Limitations

However, this study is subject to several specific limitations that may affect the interpretation of the results, which are described objectively as follows. First, the in vivo experiments were restricted to two groups: a negative control group (DMSO group) and a combination therapy group (Rapamycin + Alpelisib group), with the absence of a positive control group (e.g., Rapamycin + Ponatinib combination). This experimental design inherently limits the ability to directly compare the therapeutic efficacy of different combination regimens, as there is no reference positive treatment to benchmark the performance of the Rapamycin + Alpelisib combination. Nevertheless, the results clearly demonstrated that, compared with the negative control group, the Rapamycin + Alpelisib combination significantly inhibited lesion progression, which was mediated by the regulation of the PI3K/AKT/mTOR signaling pathway and p53 expression. To address this limitation, future studies should refine the experimental design by incorporating a positive control group, thereby enabling a more comprehensive evaluation of the therapeutic advantages of the Rapamycin + Alpelisib combination relative to other potential treatment strategies.

Additionally, to initially explore the synergistic effects of Rapamycin and Alpelisib and evaluate the therapeutic efficacy of their combination, the dose of the combination therapy was set to half of the experimental concentration used for each single drug. This approach was based on the hypothesis that the two drugs might exert synergistic effects at low doses, allowing for significant therapeutic efficacy while reducing potential toxic side effects. However, this dose selection lacks precise optimization, which may affect the accuracy of assessing the true synergistic potential and optimal therapeutic effect of the combination. Although the current results confirmed the presence of synergistic effects between the two drugs, future studies should further optimize the combination dose by calculating the combination index (CI), which will help to accurately determine the optimal ratio of the two drugs and further improve the therapeutic efficacy and safety of the combination therapy. Furthermore, future studies should conduct more systematic and large-scale in vivo animal experiments to further validate the long-term therapeutic efficacy, biosafety, and in vivo pharmacodynamic mechanisms of this combination regimen, so as to provide more solid experimental evidence for its potential clinical transformation.

6. Conclusions

The overactivation of the PI3K pathway drives venous malformations. This study reveals that Rapamycin and Alpelisib synergistically inhibit PI3K and activate P53, offering significant therapeutic potential for venous malformations.

Availability of Data and Materials

All data generated or analyzed during this study are included in this article. For further inquiries, please contact the corresponding author directly.

Author Contributions

YL and YH conceived and designed the experiments, performed the experiments, collected the data, and drafted the manuscript; JL, TW, and WW performed part of the experimental operations, collected and analyzed some of the data; ZCT conceived and designed the experiments, provided experimental guidance, analyzed the experimental data, translated the manuscript, and revised it critically. All authors read and approved the final manuscript. All authors have participated sufficiently in the work and agreed to be accountable for all aspects of the work. All authors contributed to editorial changes in the manuscript.

Ethics Approval and Consent to Participate

All pathological tissue sections of venous malformations (VMs) were provided by the Department of Pathology at the First Affiliated Hospital of Kunming Medical University. We have signed a scientific research cooperation agreement with the Department of Pathology at the First Affiliated Hospital of Kunming Medical University and submitted the approval document (Approval No.: KHLL2023-KY198) from the Medical Ethics Committee of the First People's Hospital of Yunnan Province. All gingival/skin tissues were obtained as discarded surgical materials from oral and maxillofacial surgeries at the First People's Hospital of Yunnan Province, and Human umbilical vein endothelial cells (HUVECs) were isolated from umbilical cords provided by the Obstetrics Department of the First People's Hospital of Yunnan Province, with approval from the Medical Ethics Committee of the First People's Hospital of Yunnan Province (Approval No.: KHLL2023-KY198). Human Oral Mucosal Fibroblasts (HOMFs) were kindly provided by Professor Jiemei Zhai's research group at the Affiliated Stomatology Hospital of Kunming Medical University. All experiments were conducted in strict accordance with the Declaration of Helsinki and relevant ethical guidelines and regulations, ensuring compliance with ethical requirements for human experimentation and the use of human tissue samples. Informed consent was obtained from all patients or their families, agreeing to the use of their pathological tissue sections or tissue samples for this study. The nude mice (nu/nu, Kunming Medical University Animal Research Institute, China) used in this study were purchased from the Kunming Medical University Animal Research Institute. All animal experiments were approved by the Animal Welfare Ethics Committee of Kunming Medical University (Approval No.: Kmmu20230003) and were conducted in strict compliance with principles of animal protection, animal welfare, and ethical guidelines. The study strictly adhered to the principles of Replacement, Reduction, and Refinement (3R).

Acknowledgment

We would like to express our sincere gratitude to all the individuals, institutions and fundings who contributed to this study. We sincerely acknowledge Professor Hefeng Yang, Professor Zheyi Sun, Professor Rongqiang Yang, Professor Zichao Dai, and Professor Weihong Wang from Kunming Medical University for their critical technical expertise provided during the experimental phase of this study.

Funding

This work was supported by the Yunnan Provincial Science and Technology Talent and Platform Planning Project (Grant No. 202305AF150120), and the Xingdian Talents Program Famous Medical Specialty Project (Grant No. XDYC-MY-2022-0049).

Conflict of Interest

The authors declare no conflict of interest.

Supplementary Material

Supplementary material associated with this article can be found, in the online version, at https://doi.org/10.31083/FBL48694.

References

[1] Colletti G, Ierardi AM. Understanding venous malformations of the head and neck: a comprehensive insight. Medical Oncology (Northwood, London, England). 2017; 34: 42. https://doi.org/10.1007/s12032-017-0896-3.

[2] Leyman B, Govaerts D, Dormaar JT, Meeus J, Bila M, Coropciuc R, *et al*. A 16-year retrospective study of vascular anomalies in the head and neck region. Head & Face Medicine. 2023; 19: 32. https://doi.org/10.1186/s13005-023-00376-z.

[3] Bertino F, Trofimova AV, Gilyard SN, Hawkins CM. Vascular anomalies of the head and neck: diagnosis and treatment. Pediatric Radiology. 2021; 51: 1162–1184. https://doi.org/10.1007/s00247-021-04968-2.

[4] Sadick M, Müller-Wille R, Wildgruber M, Wohlgemuth WA. Vascular Anomalies (Part I): Classification and Diagnostics of Vascular Anomalies. RoFo: Fortschritte Auf Dem Gebiete Der Rontgenstrahlen Und Der Nuklearmedizin. 2018; 190: 825–835. https://doi.org/10.1055/a-0620-8925.

[5] Gallant SC, Chewning RH, Orbach DB, Trenor CC, 3rd, Cunningham MJ. Contemporary Management of Vascular Anomalies of the Head and Neck-Part 1: Vascular Malformations: A Review. JAMA Otolaryngology– Head & Neck Surgery. 2021; 147: 197–206. https://doi.org/10.1001/jamaoto.2020.4353.

[6] Kim H, Joh J, Labropoulos N. Characteristics, clinical presentation, and treatment outcomes of venous malformation in the extremities. Journal of Vascular Surgery. Venous and Lymphatic Disorders. 2022; 10: 152–158. https://doi.org/10.1016/j.jvsv.2021.05.011.

[7] Lee WJ, Cho KR, Choi JW, Kong DS, Seol HJ, Nam DH, *et al*. Stereotactic radiosurgery for orbital cavernous venous malformation: a single center's experience for 15 years. Acta Neurochirurgica. 2021; 163: 357–364. https://doi.org/10.1007/s00701-020-04575-4.

[8] Song D, Guo L, Sheng H, Li J, Wang L, Wu C, *et al*. DSA-guided percutaneous sclerotherapy for children with oropharyn-

geal low-flow venous malformation. Experimental and Therapeutic Medicine. 2020; 19: 3405–3410. https://doi.org/10.3892/etm.2020.8581.

[9] Johnin K, Mori Y, Nakagawa S, Kobayashi K, Kageyama S, Kawauchi A. Venous malformation of the glans penis: "Every-5-mm" neodymium:yttrium-aluminum-garnet laser irradiation. International Journal of Urology: Official Journal of the Japanese Urological Association. 2021; 28: 1189–1191. https://doi.org/10.1111/iju.14662.

[10] Limaye N, Wouters V, Uebelhoer M, Tuominen M, Wirkkala R, Mulliken JB, *et al*. Somatic mutations in angiopoietin receptor gene TEK cause solitary and multiple sporadic venous malformations. Nature Genetics. 2009; 41: 118–124. https://doi.org/10.1038/ng.272.

[11] Soblet J, Limaye N, Uebelhoer M, Boon LM, Vikkula M. Variable Somatic TIE2 Mutations in Half of Sporadic Venous Malformations. Molecular Syndromology. 2013; 4: 179–183. https://doi.org/10.1159/000348327.

[12] Goines J, Li X, Cai Y, Mobberley-Schuman P, Metcalf M, Fishman SJ, *et al*. A xenograft model for venous malformation. Angiogenesis. 2018; 21: 725–735. https://doi.org/10.1007/s10456-018-9624-7.

[13] Limaye N, Kangas J, Mendola A, Godfraind C, Schlögel MJ, Helaers R, *et al*. Somatic Activating PIK3CA Mutations Cause Venous Malformation. American Journal of Human Genetics. 2015; 97: 914–921. https://doi.org/10.1016/j.ajhg.2015.11.011.

[14] Hoeger PH. Genes and phenotypes in vascular malformations. Clinical and Experimental Dermatology. 2021; 46: 495–502. https://doi.org/10.1111/ced.14513.

[15] Castillo SD, Tzouanacou E, Zaw-Thin M, Berenjeno IM, Parker VER, Chivite I, *et al*. Somatic activating mutations in Pik3ca cause sporadic venous malformations in mice and humans. Science Translational Medicine. 2016; 8: 332ra43. https://doi.org/10.1126/scitranslmed.aad9982.

[16] Le Cras TD, Goines J, Lakes N, Pastura P, Hammill AM, Adams DM, *et al*. Constitutively active PIK3CA mutations are expressed by lymphatic and vascular endothelial cells in capillary lymphatic venous malformation. Angiogenesis. 2020; 23: 425–442. https://doi.org/10.1007/s10456-020-09722-0.

[17] Jauhiainen S, Ilmonen H, Vuola P, Rasinkangas H, Pulkkinen HH, Keränen S, *et al*. ErbB signaling is a potential therapeutic target for vascular lesions with fibrous component. eLife. 2023; 12: e82543. https://doi.org/10.7554/eLife.82543.

[18] Cai Y, Schrenk S, Goines J, Davis GE, Boscolo E. Constitutive Active Mutant TIE2 Induces Enlarged Vascular Lumen Formation with Loss of Apico-basal Polarity and Pericyte Recruitment. Scientific Reports. 2019; 9: 12352. https://doi.org/10.1038/s41598-019-48854-2.

[19] Kennedy MA, Xu Z, Wu Y, Sohl CD. A Tie2 kinase mutation causing venous malformations increases phosphorylation rates and enhances cooperativity. Biochemical and Biophysical Research Communications. 2019; 509: 898–902. https://doi.org/10.1016/j.bbrc.2019.01.020.

[20] Du Z, Ma HL, Zhang ZY, Zheng JW, Wang YA. Transgenic Expression of A Venous Malformation Related Mutation, *TIE2-R849W*, Significantly Induces Multiple Malformations of Zebrafish. International Journal of Medical Sciences. 2018; 15: 385–394. https://doi.org/10.7150/ijms.23054.

[21] Castel P, Carmona FJ, Grego-Bessa J, Berger MF, Viale A, Anderson KV, *et al*. Somatic PIK3CA mutations as a driver of sporadic venous malformations. Science Translational Medicine. 2016; 8: 332ra42. https://doi.org/10.1126/scitranslmed.aaf1164.

[22] Li X, Cai Y, Goines J, Pastura P, Brichta L, Lane A, *et al*. Ponatinib Combined With Rapamycin Causes Regression of Murine Venous Malformation. Arteriosclerosis, Thrombosis, and Vascular Biology. 2019; 39: 496–512. https://doi.org/10.1161/ATVBAHA.118.312315.

[23] Nakatsu MN, Hughes CCW. An optimized three-dimensional in vitro model for the analysis of angiogenesis. Methods in Enzymology. 2008; 443: 65–82. https://doi.org/10.1016/S0076-6879(08)02004-1.

[24] Du Z, Zheng J, Zhang Z, Wang Y. Review of the endothelial pathogenic mechanism of TIE2-related venous malformation. Journal of Vascular Surgery. Venous and Lymphatic Disorders. 2017; 5: 740–748. https://doi.org/10.1016/j.jvsv.2017.05.001.

[25] Pang C, Lim CS, Brookes J, Tsui J, Hamilton G. Emerging importance of molecular pathogenesis of vascular malformations in clinical practice and classifications. Vascular Medicine (London, England). 2020; 25: 364–377. https://doi.org/10.1177/1358863X20918941.

[26] Clapp A, Shawber CJ, Wu JK. Pathophysiology of Slow-Flow Vascular Malformations: Current Understanding and Unanswered Questions. Journal of Vascular Anomalies. 2023; 4: e069. https://doi.org/10.1097/JOVA.0000000000000069.

[27] Schonning MJ, Koh S, Sun RW, Richter GT, Edwards AK, Shawber CJ, *et al*. Venous malformation vessels are improperly specified and hyperproliferative. PloS One. 2021; 16: e0252342. https://doi.org/10.1371/journal.pone.0252342.

[28] Maruani A, Tavernier E, Boccara O, Mazereeuw-Hautier J, Leducq S, Bessis D, *et al*. Sirolimus (Rapamycin) for Slow-Flow Malformations in Children: The Observational-Phase Randomized Clinical PERFORMUS Trial. JAMA Dermatology. 2021; 157: 1289–1298. https://doi.org/10.1001/jamadermatol.2021.3459.

[29] Teng, J, Martini, J, Kelly, M, *et al*. Sirolimus for Venous Malformations: A Systematic Review of Efficacy and Safety. Lymphatic Research and Biology. 2025; 23: 311–319. https://doi.org/10.1177/15578585251377562.

[30] Eng, W. Targeted Medical Therapies for Vascular Anomalies: A Clinical Review. American Journal of Medical Genetics Part C. 2025; 199: 161–175. https://doi.org/10.1002/ajmgc.70000.

[31] Freixo C, Ferreira V, Martins J, Almeida R, Caldeira D, Rosa M, *et al*. Efficacy and safety of sirolimus in the treatment of vascular anomalies: A systematic review. Journal of Vascular Surgery. 2020; 71: 318–327. https://doi.org/10.1016/j.jvs.2019.06.217.

[32] Durán-Romero AJ, Hernández-Rodríguez JC, Ortiz-Álvarez J, Domínguez-Cruz JJ, Monserrat-García MT, Conejo-Mir Sánchez J, *et al*. Efficacy and safety of oral sirolimus for high-flow vascular malformations in real clinical practice. Clinical and Experimental Dermatology. 2022; 47: 57–62. https://doi.org/10.1111/ced.14841.

[33] Sterba M, Pokorna P, Faberova R, Pinkova B, Skotakova J, Seehofnerova A, *et al*. Targeted treatment of severe vascular malformations harboring PIK3CA and TEK mutations with Alpelisib is highly effective with limited toxicity. Scientific Reports. 2023; 13: 10499. https://doi.org/10.1038/s41598-023-37468-4.

[34] Zerbib L, Ladraa S, Fraissenon A, Bayard C, Firpion M, Venot Q, *et al*. Targeted therapy for capillary-venous malformations. Signal Transduction and Targeted Therapy. 2024; 9: 146. https://doi.org/10.1038/s41392-024-01862-9.

[35] Chen M, Choi S, Wen T, Chen C, Thapa N, Lee JH, *et al*. A p53-phosphoinositide signalosome regulates nuclear AKT activation. Nature Cell Biology. 2022; 24: 1099–1113. https://doi.org/10.1038/s41556-022-00949-1.

[36] Si Y, Huang J, Li X, Fu Y, Xu R, Du Y, *et al*. AKT/FOXO1 axis links cross-talking of endothelial cell and pericyte in TIE2-mutated venous malformations. Cell Communication and Signaling: CCS. 2020; 18: 139. https://doi.org/10.1186/s12964-020-00606-w.